Eng. Sci., 2020, 11, 44-53

Engineered Science

DOI: https://dx.doi.org/10.30919/es8d1120

Deployment Analysis of Aramid Fiber Reinforced Shape Memory Epoxy Resin Composites

Xianghai Jing,[1,3] Jianzheng Wei,[2,*] Yuxi Liu,[3] Bo Song,[2] and Yuyan Liu[1]

Abstract

This work aims to study the shape recovery of aramid fiber-reinforced shape-memory epoxy resin composite (SMERs). A circular tube can be assumed to be composed of a pair of curved tape with the same radius before being folded, and the middle position of this tubular structures is folded with a small curvature. The cylindrical shell is deformed into a flat shape at the folding line. So the shape memory fold-deploy experiments of the three deployable structures, flat tape, curved tape, and circular tube prepared with SMERs, were performed respectively, and the shape memory deployable processes were also simulated with finite element model. The temperature dependences of deployment angle, axial stress and axial strain in the shape memory folding step, cooling step, constraint removal step and reheating step were analyzed. The results showed that the full deployable process of each deployable structure was simulated well compared with experimental results. The strength failure in structure component occurred during the fold-deploy shape memory process. The long-term shear modulus of viscoelastic materials had a great influence on shape memory performance.

Keywords: Shape-memory composite; Epoxy resin; Fold-deploy; Viscoelasticity; Finite element analysis.
Received: 11 May 2020; Accepted: 27 July 2020.
Article type: Research article.

1. Introduction

The shape-memory polymers (SMPs) have the advantages of low density, excellent shape-recovery capacity, electrical insulation, easy processability, and low cost.[1-5] Thus, SMPs are widely used in electronics, aircraft, and aerospace fields, such as in actuators and self-deployable space structures.[6-10] An SMP shifts between rigid and elastic states through thermal stimuli at the critical temperature (T_c).[11] The polymer is deformed to a desired shape at a temperature above T_c. Then, the SMP is held in its final shape and cooled below T_c. After cooling, the constraint is removed from the SMP, which holds the deformed shape. Finally, the SMP is heated above T_c to recover the original undeformed as-processed shape.[12-15] The driving factor of shape-recovery performance is the elastic strain generated in deformation process.[16-18]

An accurate thermal mechanical constitutive theory to predict the deformation and recovery of SMP is required to develop the simulation capacity for the design of devices, such as the self-deployable space structures, especially for the circular tube that was seldom studied in the previous research. In recent years, several efforts at constitutive modeling of the thermo-mechanical response of SMPs have been published.[19-23] Other significant works on finite element analysis of SMPs have also been published.[11,24–29] A framework for glassy SMPs (GSMPs) using the notion of natural configuration of a material taking into account the thermal expansion of polymers was presented, and the corresponding finite element (FE) model for GSMP using user subroutine was developed.[11] Diani et al.[20] proposed a 3D thermoviscoelastic model for the thermomechanical behavior of SMPs. Yang et al.[24] developed an FE model based on the viscoelastic theories of polymer to simulate the shape-memory process of SMPs and obtain the relationships between stress–temperature and strain–temperature. Most of the previous studies were focused on the FE modelling of beam structure, plate structure, shell structure and hinge. The finite element analysis of SMP circular tube structure has not been reported. However, the circular tube structure is actually widely applied, such as the shape memory supporting tube in the large antenna structure. The reason

[1] *School of Chemical Engineering and Technology, Harbin Institute of Technology, Harbin 150001, China .*
[2] *National Key Laboratory of Science and Technology on Advanced Composites in Special Environment, Harbin Institute of Technology, Harbin 150080, China*
[3] *School of Material Science and Chemical Engineering, Chuzhou University, Chuzhou 239000, China.*
**E-mail: weijz@hit.edu.cn (J. Wei).*

for the lack of research on the SMP circular tube is that the heating factor needs to be included in the FE model, besides, the stresses of upper and lower surface after folding for the tube are different. Therefore, the finite element analysis of the SMP circular tube is very complicated.

This paper studies the fold-deploy behavior of shape-memory epoxy resin (SMER) composite with the circular tube. The most critical issue is how the cross-sectional shape of the tube at the folding line is deformed. Fig. 1 shows how the Z-folded SMER composite tube deformed. As shown in Fig.1, the circular tube can be assumed to be composed of a pair of curved tape with the same radius before being folded, and the middle position of this tubular structures is folded with a small curvature. The cylindrical shell is deformed into a flat shape at the folding line. Therefore, the flat tape and curved tape with SMER composite were first studied, then the circular tube. An FE model based on the viscoelastic theory was created to evaluate the strains and stresses of SMER composite during the whole shape memory process. The fold-deploy experiment of SMER composite was also performed. The simulated results are compared with the experimental results. The influence of key parameter to recovery rate is discussed.

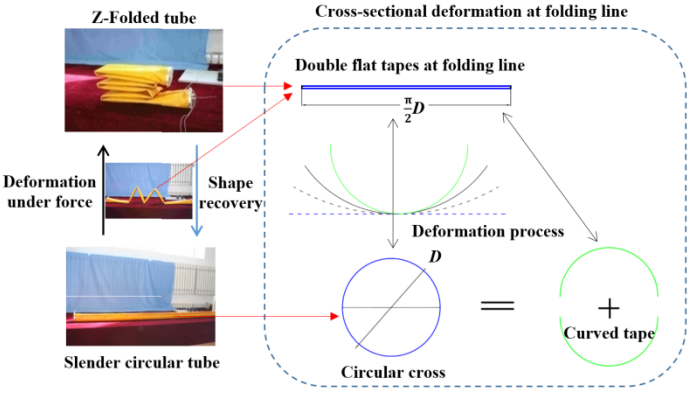

Fig. 1 The fold-deploy behavior of shape-memory epoxy resin (SMER) composite with the circular tube.

2. Experimental section

2.1 Material

Epoxy resin was constituted of the following components: E51 (liquid epoxy resin, Bluestar New Chemical Materials Co., Ltd, China), triethylenetetramine (hardener, Tianjin Tianda Chemical Reagent Co., China), octylamine (toughening agent, J&K Scientific). Kevlar® 49 fiber plain-weave (240 g/m^2 weight, 1500D for both warp and weft) was produced by DuPont. Polyimide film (25 μm thickness) was purchased from Tianjin Taiyuan Electronic Material Co., Ltd, China.

2.2 Preparation of deployable structures with SMER composite

The SMER composite was made of the Kevlar® 49 fiber plain-weave laminated with epoxy resin, and the resin content was controlled as 40 wt.%. The innermost layer was the polyimide film with heating wires, the laying way of the heating wires and fabric is shown in Fig. 2. The heating wires were laid by using the graph paper to control the distance between two wires. The heating wires at the two ends of the composite tape or tube were connected with thermocouple, so that the composite can perform the entire shape-memory process through thermocouple heating.

2.3 Folding radius design

The key issue on recoverable deployment is how the cross-sectional shape of the SMER tube at the folding line is deformed, and this is closely related to the folding radius to be designed. Here, two samples were taken from the bended regions of the composite specimens. The morphologies of the specimen surface were further examined by scanning electron microscopy (SEM, Model FEI Quanta 200, USA). Images were obtained by secondary electrons at 20 kV. The samples were gold–palladium coated according to the standard technique to limit the charging effect**.** Fig. 3 showed that when the SMER composites were folded with the radius of 0 mm and 4 mm, there was only the resin matrix partially broken, but the reinforcement fiber had no obvious damage. The smaller the folding radius, the more obvious the width of the crack at the folding line. When the elastic modulus of the material is unchanged and the same stress state exists at the initial folding, the larger the crack width at the folding line, the greater the elastic strain energy released according to the Griffith fracture theory. For the circular tubes made by SMER material, the smaller the radius of curvature of the fold, the greater the elastic strain energy released by the formation of cracks. Energy for the transition from the condensed phase to the free phase is produced in the SMER material by heating to the glass transition temperature (T_g). That's to say, it can be concluded that the smaller the radius of fold curvature according to the conservation of energy, the more serious the damage to the material and the greater the corresponding fracture energy. Therefore, the larger the radius of curvature of the shape memory recoverable force, the greater the corresponding deployable torque. In short, in the deployable test on SMER tube, the radius of the circular at the folding line was determined to be 10 mm.

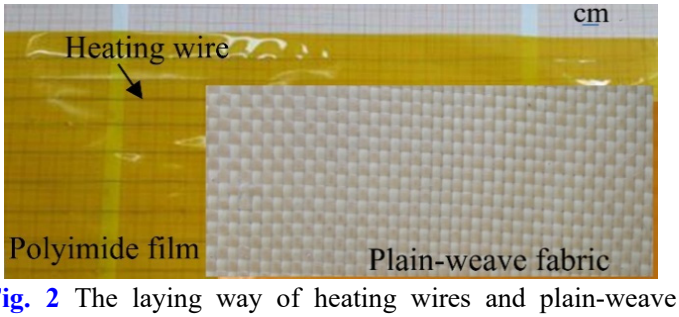

Fig. 2 The laying way of heating wires and plain-weave fabric.

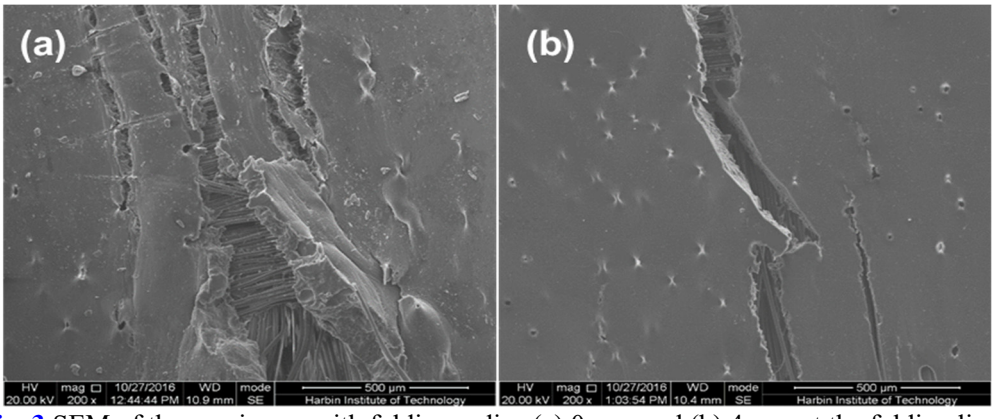

Fig. 3 SEM of the specimens with folding radius (a) 0 mm and (b) 4 mm at the folding line.

2.4 Fold-deploy experiments

To investigate the deployment process of the composites, the experimental method of evaluating shape memory properties of the epoxy resins was performed as reported by our previous work.[30] The cured specimen was heated to about 120 °C and deformed to a "U" shape by a 2 cm diameter cylinder at the folding line, then cooled to room temperature about 20 °C to fix the deformation. The fixed states of three types of specimens for deployment tests are shown in Fig. 4. The material properties of the three specimens are given in Table 1. The length, thickness and density were almost the same. Here, the same diameter of the curved tape and circular tube was chosen as 4.5 cm, and width of the flat tape was designed as $4.5\pi/2$, i.e. 7.1 cm. The circular tube was unable to bend to initial angle 0°, therefore, an initial angle 30° was applied for it. Subsequently, the deformed polymer was heated to about 120 °C, and the recovery process was recorded when the recovery angle was 30°, 60°, 90°, 120°, 150°, and 180°.

2.5 Differential scanning calorimetry test

The differential scanning calorimetry (DSC) test was performed on a Mettler DSC-1 analyzer (Columbus, Ohio, USA) for T_g characterization of the epoxy resin. The T_g value of the cured resin was investigated at a heating rate of 10 °C min^{-1} from 20 °C to 140 °C.

3. Results and discussion

3.1 Numerical method of SMER composite

Nonlinear dynamic deployment is simulated using the measured dimensions of the experimental specimens to study the dynamic mechanical properties of SMER composite during the whole shape memory process. Firstly, viscoelasticity of SMER material is analyzed, and finite element model is also created according to the test results of DSC. Then loading steps and boundary condition are adopted to make only half of the model deploy freely.

Table 1. Material properties of the specimens for deployment experiments.

Parameter	Flat tape	Curved tape	Circular tube
Length (cm)	50	50	50
Thickness t (mm)	0.48	0.49	0.47
Width/Diameter d (cm)	7.1	4.5	4.5
Density (kg m^{-3})	831	838	841
Curvature radius after folding (cm)	1	1	1
Initial angle (°)	0±2	0±2	30±2

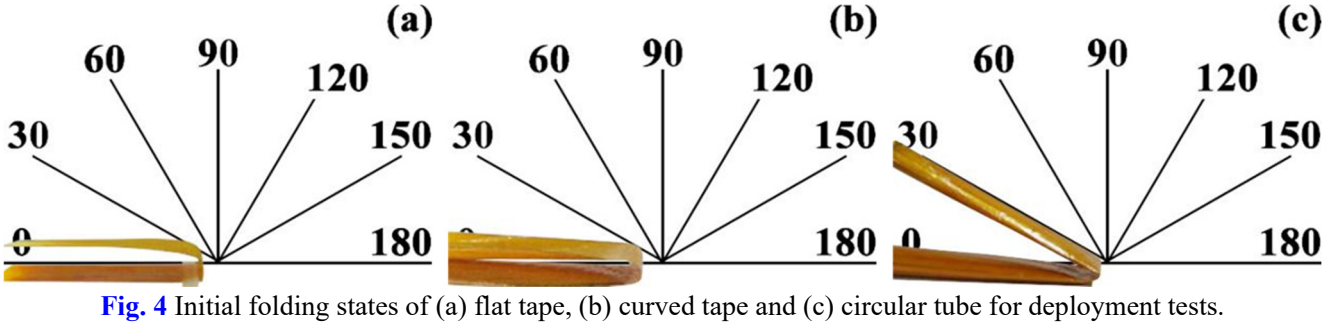

Fig. 4 Initial folding states of (a) flat tape, (b) curved tape and (c) circular tube for deployment tests.

3.1.1 Viscoelastic analysis

Constitutive models are critical to predict the deformation and recovery of the SMPs under constraints. Viscoelastic theory is introduced into the finite element analysis (FEA). The constitutive model for linear isotropic viscoelasticity is as follows:

$$\sigma(t) = \int_0^t 2G(\tau - t')\dot{e}dt' + I\int_0^t K(\tau - t')\dot{\varphi}dt' \quad (1)$$

Here, $\dot{e}$ and $\dot{\varphi}$ are the mechanical deviatoric and volumetric strains; K is the bulk modulus and G is the shear modulus, which are functions of the reduced time τ; and the dot denotes differentiation with respect to t'.

The reduced time is related to the actual time through the integral equation,

$$\tau = \int_0^t \frac{dt'}{A_T(T(t))} \quad (2)$$

where T is the temperature and A_T is the shift function. A commonly used shift function is the Williams–Landel–Ferry (WLF) equation,[31] which has the following form:

$$\log A_T = \frac{-C_1^g(T - T_g)}{C_2^g + T - T_g} \quad (3)$$

where C_1^g and C_2^g are constants and T_g is the glass transition temperature. This is the temperature at which, in principle, the behavior of the material changes from glassy to rubbery. If $T \leq T_g - C_2^g$, deformation changes will be elastic.

The relaxation functions $K(t)$ and $G(t)$ can be defined individually in terms of a series of exponentials known as the Prony series[32]:

$$K(t) = K_\infty + \sum_{i=1}^{n_K} K_i e^{-t/\tau_i^K} \quad (4)$$

$$G(t) = G_\infty + \sum_{i=1}^{n_G} G_i e^{-t/\tau_i^G} \quad (5)$$

where K_∞ and G_∞ represent the long-term bulk and shear modulus. Generally, the relaxation times τ_i^K and τ_i^G need not equal each other; however, the numerical method assumes that $\tau_i = \tau_i^K = \tau_i^G$, and the number of terms in bulk and shear, n_K and n_G, need not be equal. In fact, in many practical cases n_K = 0 can be assumed. Hence, the equations for the volumetric terms can be derived in an analogous way.

The relaxation functions $K(t)$ and $G(t)$ can also be expanded in a Prony series in terms of relative modulus,

$$\frac{K(t)}{K_0} = 1 - \sum_{i=1}^{n_K} k_i^p (1 - e^{-t/\tau_i^K}) \quad (6)$$

$$\frac{G(t)}{G_0} = 1 - \sum_{i=1}^{n_G} g_i^p (1 - e^{-t/\tau_i^G}) \quad (7)$$

$$k_i^p = \frac{K_i}{K_0} \quad (8)$$

$$g_i^p = \frac{G_i}{G_0} \quad (9)$$

where K_0 and G_0 represent the instantaneous bulk modulus and instantaneous shear modulus, respectively. k_i^p and g_i^p represent the relative bulk modulus and relative shear modulus, respectively.

3.1.2 FEA model

According to the test results of DSC, the T_g value of the cured resin was 78 °C. The constant in WLF equation and the viscoelastic parameters used in this FE Model are based on published literature.[24] The parameters in the Prony equation and WLF equation are shown in Tables 2–4.

Table 2. Viscoelastic parameters in the Prony equation.

	Relative shear modulus g_i^p	Reduced time τ (s)
1	0.478	6.890
2	0.344	0.650
3	0.052	0.100
4	0.057	0.030
5	0.040	0.013
6	0.028	0.097
Total	0.999	

Table 3. Viscoelastic parameters at glass transition temperature T_g.

Instantaneous relaxation modulus E_0 (MPa)	Long-term elastic modulus E_∞ (MPa)	Instantaneous Poisson's ratio v_0	Thermal expansion coefficient A (1 °C^{-1})
146	0.146	0.4	6.47×10^{-5}

Table 4. Viscoelastic parameters in WLF equation.

T_g	C_1	C_2
78	15.6	32.6

The SMER composite specimen is a thin-walled composite structure; hence, the shell element was used in the FE Model. The model was meshed using a 4-node, quadrilateral, shell element (S4R) with reduced integration and a large-strain formulation. The meshed models for three types of specimens are shown in Fig. 5. The model length is 50 cm.

3.1.3 Loading steps and boundary conditions

The periodic boundary conditions applied on the SMP FE model are shown in Table 5. The shape memory FEA includes four steps, i.e. the bending process, the cooling process, the shape fixity, and the recovering process. The "encastre" boundary condition is adopted to make only half of the model deploy freely. The application of bending displacement to the other end of the model for folding the specimen is shown in Fig. 6.

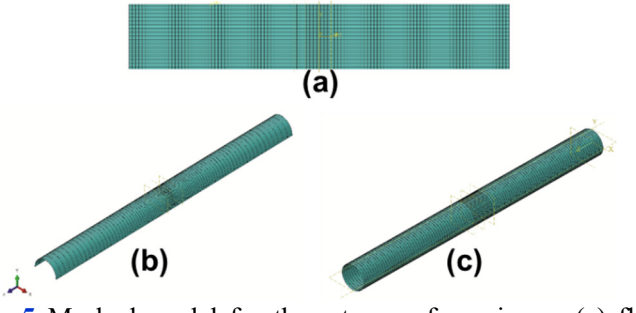

Fig. 5 Meshed model for three types of specimens (a) flat tape, (b) curved tape, and (c) circular tube.

3.2 Numerical simulation analysis of the shape memory process

3.2.1 Flat tape

To study the shape memory deployable process of the circular tube, the FEA analyses of the flat tape and curved tape are the basis. The second and third columns of Table 6 shows the FEA results and the experimental deployable process of flat tape deployed to 30°, 60°, 90°, 120°, 150° and 180°. The element located at the symmetry bending region is selected to check the variation of axial stress and strain, as shown in Table 6. The FEA and the experiment results show that the deployment angle with shape-memory recovery and the deformation at the folding line are consistent, which verifies the correctness of the simulation method.

The variations of temperature, deployment angle, strain, and stress during the whole shape memory process are shown in Fig. 7. Step number "①"–"④" represents the folding step, cooling step, constraint removal step and reheating step, respectively.

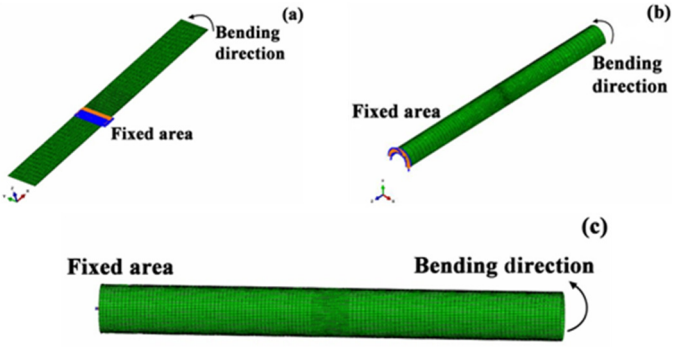

Fig. 6 Boundary conditions of FE models for three types of specimens: (a) flat tape, (b) curved tape, and (c) circular tube.

Table 5. Analysis steps and loading conditions for finite element model.

Step No.	Step time (s)	Boundary and load conditions	Corresponding shape memory process
Initial State		Set the initial temperature (T_h) as 120 °C; fix one end of the specimen.	The specimens were heated to 120 °C, which made them soften.
①	10	Apply bending displacement to the other end of the specimen. For tube, make a dent at top point before bending.	Apply bending displacement at 120 °C, the specimens were bended to U type.
②	10	The temperature decreased from 120 °C to 20 °C linearly to cool down the specimens.	The specimens were cooled down to 20 °C without removing the external force.
③	10	Maintain the temperature (T_b) at 20 °C. Free the bending restraint.	The external force was unloaded, and the shape of the specimens were fixed.
④	10	Heating the specimen up linearly from 20 °C to 120 °C to make the specimen dynamically recover.	The specimens were heated from room 20 °C to 120 °C and dynamic recovery occurred.

Table 6 Recovery process of the flat tape and curved tape at deployment angle 0°, 30°, 60°, 90°, 120°, 150°, and 180°.

Deployment angle	Recovery process of flat tape		Recovery process of curved tape	
	FEA	Experiment	FEA	Experiment
0°	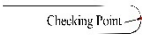	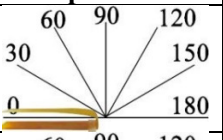		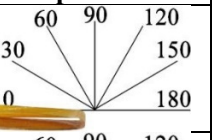
30°	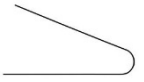	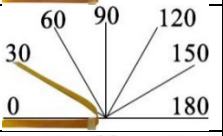		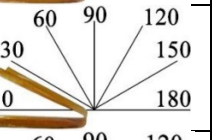
60°	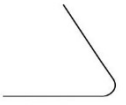	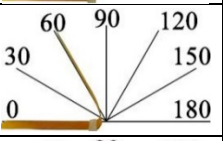	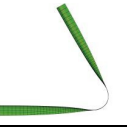	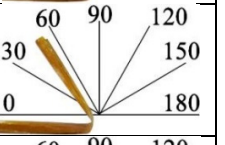
90°	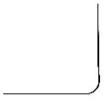	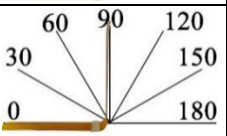		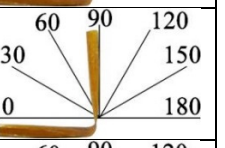
120°		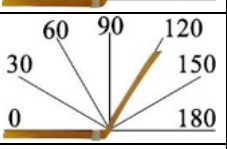		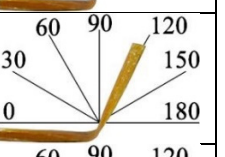
150°		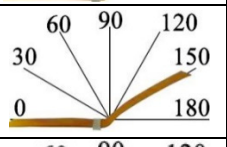		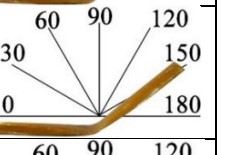
180°		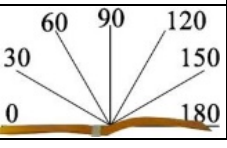		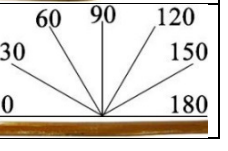

As shown in **Fig. 7a**, the temperature keeps at T_h = 120 °C during the step ①, and the flat tape is folded from 180° to 0°. The axial strain and axial stress on surface $z = -t/2$ of the flat tape are shown in **Fig. 7b** and **Fig. 7c**. Only the strains and stresses on the bottom surface are given, because the distributions of strains and stresses on the opposite surface are essentially identical. The axial strain and axial stress gradually increase during the bending process. The ratio of stress to strain is close to the long-term relaxation modulus, because the instantaneous relaxation modulus will decay to long-term relaxation modulus quickly when the temperature is 120 °C.

During the step ②, the flat tape is folded completely and still constrained by boundaries. With the decrease of temperature, the strain at the symmetry bending region decrease linearly. The stress increases gently with the decrease of temperature when the temperature is above T_g, while the stress increases rapidly when the temperature is below T_g. The reason is that the material transforms from high-elastic state to glassy state when the temperature is below T_g, thus the elastic modulus of material increases rapidly, leading to the quick increase of the stresses.

During the step ③, the folding constraint of flat tape is removed at low temperature T_b = 20 °C. The flat tape displays rebound after constraint removal due to the increase of elastic modulus and thermal contraction. As shown in Fig. 7a, the angle rebounds from 0° to 0.3°. The fixed rate of strain (R_f) is introduced to describe the ability of shape fixity of SMER composite, which can be obtained using the following formula:

$$R_f = \frac{\theta_f}{\theta_{max}} \times 100\% \tag{10}$$

where, θ_f is the folding angle after step ③, θ_{max} is the initial folding angle, i.e. 180°. The fixed rate of strain for the flat tape was calculated to be 99.8%. The stress leap of the flat tape at the beginning of the unconstrained process is due to the uneven stress caused by free-boundary condition in the y-direction, as shown in Fig. 8.

During the step ④, the strain initially increases linearly because of the thermal expansion at the temperature below T_g, and there is no deployment occurred. When the material is heated to a temperature above T_g, the Brownian movement of the reversible phase is activated, then the tape begins to deploy and recovers to the initial state in which the stresses and strains are zero. After the shape recovery is completed, the strain increases again owing to thermal expansion.

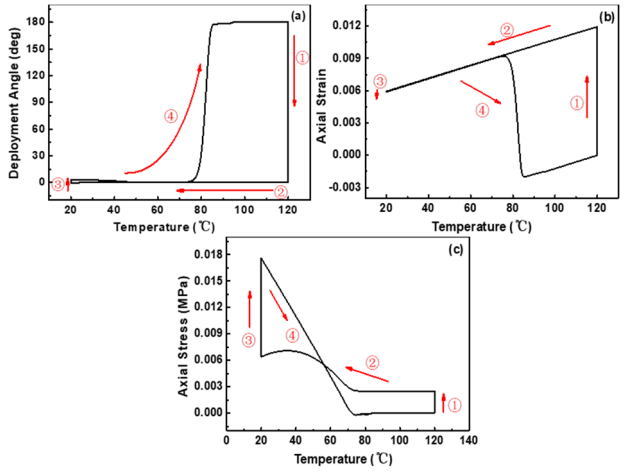

Fig. 7 Mechanical response and deployment angle variation of flat tape during shape memory deployment process: (a) deployment angle vs. temperature, (b) axial strain vs. temperature, (c) axial stress vs. temperature.

3.2.2 Curved tape

The fourth and fifth columns of Table 6 show the experimental deployable process and the FEA results of curved tape deployed to 30°, 60°, 90°, 120°, 150° and 180°. The FEA and the experiment results show that deployment angle and deformation at the folding line are consistent by shape-memory recovery. Moreover, the deformation of two kinds of tape at the folding line remains consistent before deployment angle 150°. This shows the semi-cylindrical shape tape deployed from 0 to 150° stage mainly has the performance of rotation recovery of the flat tape; the curvature radius of the curved tape returns to 45mm after 150°.

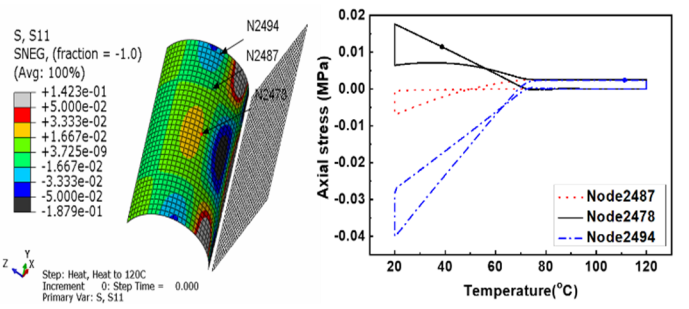

Fig. 8 Stress variation of flat tape in the bending region.

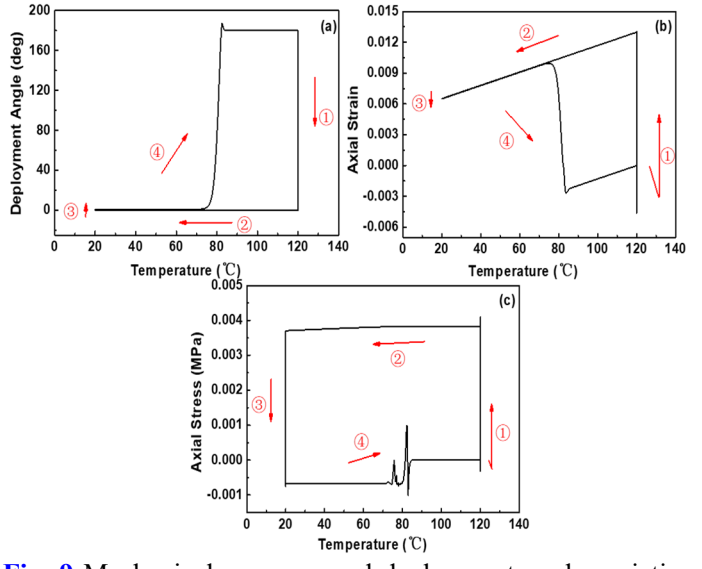

Fig. 9 Mechanical response and deployment angle variation of the curved tape during shape memory deployment process: (a) deployment angle vs. temperature, (b) axial strain vs. temperature, (c) axial stress vs. temperature.

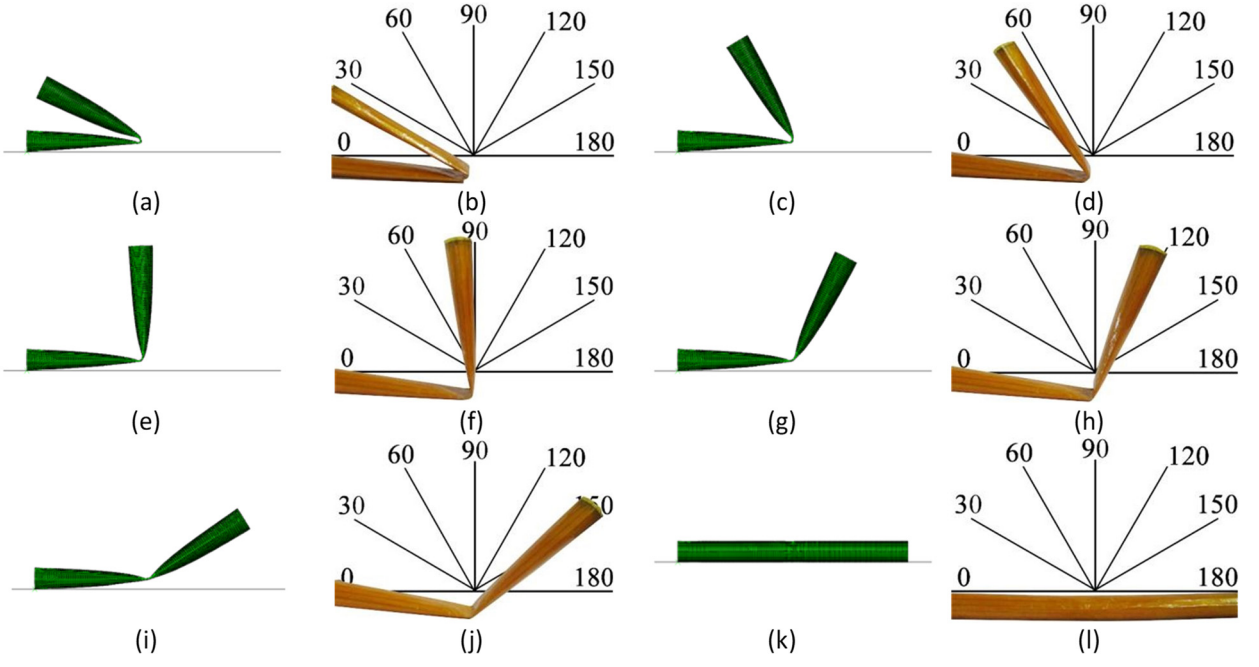

Fig. 10 Recovery process of circular tube at (a,b) initial state, (c,d) θ= 30°, (e,f) θ = 60°, (g,h) θ = 90°, (i,j) θ = 120°, (k,l) θ = 150°, and (m,n) θ = 180°.

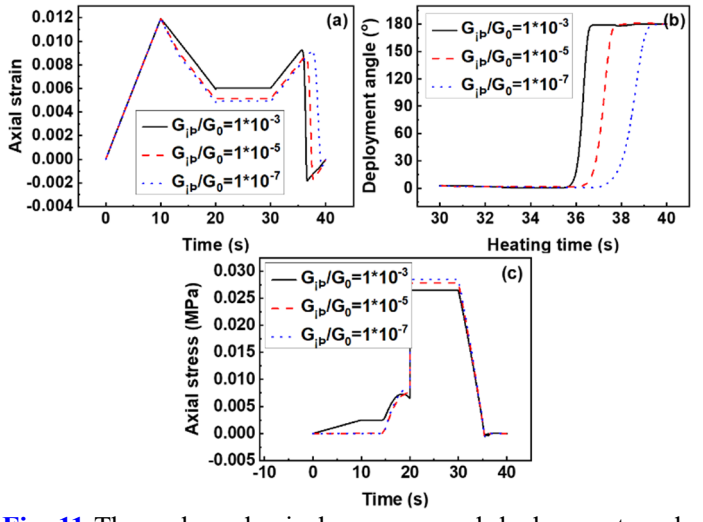

Fig. 11 Thermal mechanical response and deployment angle variation of circular tube during shape memory deployment process: (a) deployment angle vs. temperature, (b) axial strain vs. temperature, (c) axial stress vs. temperature.

Fig. 9 shows the relevant parameters of the curved tape in the whole shape memory process. As shown in Fig. 9, during the folding process (step ①), the curved tape is bended from 180° to 0°. At the beginning, the axial strains at the bottom surface of the symmetry bending region is the compression strains due to the bending of the whole curved tape, and then shifts to tension strains because of local bending. The stresses show the same trend as the strains due to bending. During the cooling process (step ②), the strain linearly decreases as the temperature decreases, whereas the stress remains almost the same due to the effect of increasing elastic modulus. During step ③, the axial stress decreases due to constraint removal, and becomes compression stress which results from the uneven stress as a free-boundary condition in the *y*-direction, similar to that for flat tape.

The fixed rate of strain of curved tape after shape fixity is 99.6%. The changes of parameters during the heating step ④ are the same with that of flat tape. Because the T_g value of the cured resin was 78 °C, SMP is undergoing the transition from the glassy state to the highly elastic state, when the temperature reaches about 80 °C during the reheating step ④. The chain molecules are dominant, and the movement between the molecules continuously overcomes the intermolecular forces. The axial stress stored at the local bending is also continuously released as its deployable deformation. Hence, the axial stress appeared fluctuation around 80°C in Fig. 9c.

3.2.3 Circular tube

The circular tube can be considered as two symmetric curved tapes with the same diameter. Fig. 10 shows the experimental deployable process and the FEA results of the circular tube deployed to 30°, 60°, 90°, 120°, 150° and 180°. The FEA and the experiment results further verify that deployment angle and deformation at the folding line are consistent by shape-memory recovery. Moreover, the deformation of three kinds of thin-wall structures at the folding line remains consistent before deployment angle 150°. The circular tube deployed from 0 to 150° also has the performance of rotation recovery of the flat tape; the curvature radius of the tube returns to 45mm after 150°.

The thermal mechanical response and deployment angle during the whole shape memory process are extracted from FEA results, as shown in Fig. 11. The inner surface of the tube located at the symmetry bending region is selected. As shown in Fig. 11b, during the folding process (step ①), the axial strain in the inner surface of the tube is under tension because of a local dent, and then decrease as a result of the tube bending. The other variations of the relevant parameters have the same trend as that of curved tape.

By comparison of the strain, stress and deployment angle variation of the three types of samples, it can be found that their overall trends were basically the same during the shape memory process. However, because the local bending and integral bending occurred during the folding process for the curved tape and the circular tube, their variations of strain were different from the flat tape, the strain of which was increased linearly. The internal axial stress of the three types of samples were also different. The reasons into the mechanism that causes the differences are as follows. When the temperature drops below T_g during the cooling stage ②, the shrinkage effect on strain causes a continuous decrease. The change of stress can be divided into two parts. Firstly, the SMP is still in a high elastic state and the elastic modulus is very small when the temperature has not been reduced to T_g. So the stress decreases slowly. Secondly, SMP begins the phase transition process when the temperature drops to T_g, and the elastic modulus increases significantly, so the change of the axial stress is obvious.

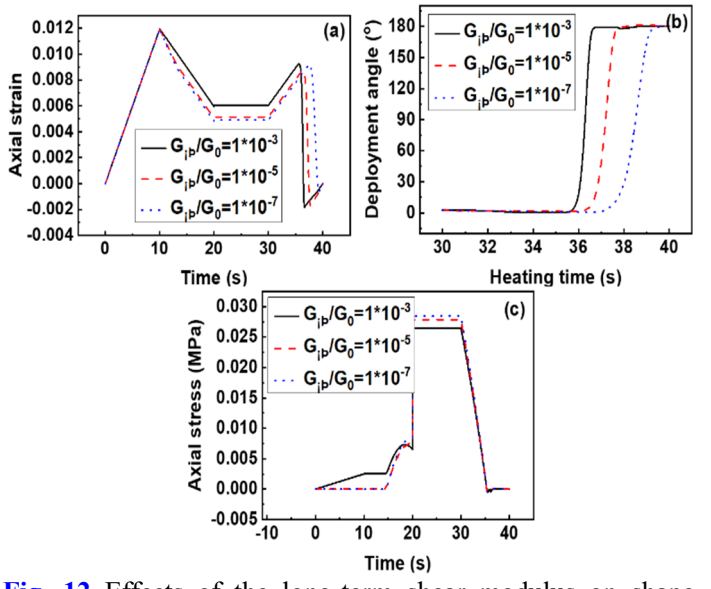

Fig. 12 Effects of the long-term shear modulus on shape memory process: (a) axial strain vs. time, (b) deployment angle vs. time, (c) axial stress vs. time.

In Fig. 7c, there is axial stress on surface z = -t/2 on the outside of the flat tape. The axial stress yields tensile state, and the value increases as the temperature decreases. In Fig. 9c, the axial stress, on surface z = -t/2 on the outside of the curve tape, yields the axial tensile and compression coupling in the hoop direction. The value changes slowly as the temperature decreases. In Fig. 11c, the axial stress on surface z = -t/2 inside curve tape of the tube represents the axial compressive state, the value increases as the temperature decreases. When the temperature reaches to 120 °C during the reheating step ④, SMP is undergoing the transition from the glassy state to the highly elastic state. The chain molecules are dominant, and the movement between the molecules continuously overcomes the intermolecular forces. The axial stress stored at the local bending is also continuously released as its deployable deformation. Finally, the stress relaxes, and the stress state of the SMP returns to the initial zero stress. In addition, the circular tube is easier to fail locally during folding process than curved tape and flat tape because of the larger local bending. Therefore, it is necessary to notice the influence of folding mode on the deployment process of tubular structure.

3.3 Viscoelasticity parameter analysis

The material parameters have a big impact on the deploy process of SMER composite. In this paper, the sensitivity analysis is presented to discover the effect of elastic modulus on the shape memory process. According to the deployment pictures in Fig. 8 and Fig. 10, it is found that the curved tape and circular tube display the characteristic of the flat tape at the bending regions. Therefore, the viscoelasticity parameter analysis is performed using the FE model of the flat tape.

The long-term shear modulus (G_∞) cannot be zero in the simulation, meaning that $\sum_{i=1}^{n_K} g_i^p < 1$. Three different relative shear modulus G_∞/G_0 were selected to study the effect of G_∞ on deploy process while keeping G_0 constant. As shown in Fig. 12b, a lower long-term shear modulus leads to a longer deployment process, because the long-term shear modulus is the driving force of the recovery. The difference of strain in the cooling step may be caused by boundary conditions. With the decrease of long-term shear modulus, the stress during the bending step scales down, as shown in Fig. 12c, because elastic modulus relaxes quickly from instantaneous modulus at high temperature, and the ratio of stress to strain is close to the long-term modulus.

4. Conclusions

The fold-deploy behavior was studied by FE method for a circular tube made of SMER composite in this paper. The circular tubular structure was decoupled into two types of flat tape and curved tape at the fold line for comparative analysis. The FE model based on viscoelastic theory was used to simulate the fold-deploy shape memory process. The FEA and the experiment results verify that deployment angle and deformation at the folding line are consistent by shape-memory recovery. In particular, the FE model was used to analysis the relationships between deployment angle and temperature, stress and temperature, strain and temperature, respectively. The results indicated that the strength failure in structure component during the fold-deploy shape memory process. The fixed rates of strain were obtained by the FE model based on SMER viscoelastic. The study of viscoelasticity parameters showed that the long-term modulus corresponding to the stationary phase was the driving force of recovery, and the viscosity corresponding to the reversible phase was the resistance of recovery.

Acknowledgements

This work was supported by the National Natural Science Foundation of China (NSFC Grant no.51573035) and Science Foundation of the National Key Laboratory of Science and Technology on Advanced Composites in Special Environments.

Supporting information

Not applicable.

Conflict of interest

There are no conflicts to declare.

References

[1] X. Li, W. Liu, Y. Li, W. Lan, D. Zhao, H. Wu, Y. Feng, X.He, Z. Li, J. Li, F. Luo, H. Tan, *J. Mater. Chem. B*, 2020, **8**, 5117-5130, doi: 10.1039/D0TB00798F.

[2] M. R. Pfau, K. G. McKinzey, A. A. Roth, M. A. Grunlan, *Biomacromolecules*, 2020, **21**, 2493-2501, doi: 10.1021/acs.biomac.0c00454.

[3] W. Wang, F. Wang, C. Zhang, Z. Wang, J. Tang, X. Zeng, X. Wan, *ACS. Appl. Mater. Inter.*, 2020, **12**, 25233-25242, doi: 10.1021/acsami.9b13316.

[4] S. Jafari, M. Nourany, M. Zakizadeh, A. Taghilou, H. A. Ranjbar, F. Noormohammadi, *Compos. Commun.*, 2020, **19**, 194-202, doi: 10.1016/j.coco.2020.03.016.

[5] M. A. Maleki-Bigdeli, M. Baniassadi, K. Wang, M. Baghani, *J. Intel. Mat. Syst. Str.*, 2020, **31**, 1465-1476, doi: 10.1177/1045389X20924837.

[6] A. Kausar, *Polym-Plast. Tech. Mat.*, 2020, **59**, 765-779, doi: 10.1080/25740881.2019.1695268.

[7] A. Kausar, *J. Plast. Film Sheet.*, 2020, **36**, 151-166, doi: 10.1177/8756087919865296.

[8] Q. Tan, F. Li, L. Liu, Y. Liu, X. Yan, J. Leng, *J. Intel. Mat. Syst. Str.*, 2019, **30**, 2688-2696, doi: 10.1177/1045389X19873398.

[9] D. Wang, L. Li, B. Zhang, Y. Zhang, M. Wu, G. Gu, Q. Ge, *Int. J. Solids Struct.*, 2020, **199**, 169-180, doi: 10.1016/j.ijsolstr.2020.04.028.

[10] Y. Zheng, B. Zeng, L. Yang, J. Shen, S. Guo, *Ind. Eng. Chem. Res.*, 2020, **59**, 2977-2987, doi: 10.1021/acs.iecr.9b06247.
[11] K. Mahesh, Constitutive Modeling of Glassy Shape Memory Polymers, New Jersey Institute of Technology, Newark, 2010.
[12] Q. Ni, C. Zhang, Y. Fu, G. Dai, T. Kimura, *Compos. Struct.*, 2007, **81**, 176-184, doi: 10.1016/j.compstruct.2006.08.017.
[13] R. K. Gupta, S. A. R. Hashmi, S. Verma, A. Naik, P. Nair, *J. Mater. Eng. Perform.*, 2020, **29**, 205-214, doi: 10.1007/s11665-020-04568-5.
[14] D. Pandit, S. M. Srinivasan, *J. Intel. Mat. Syst. Str.*, 2020, **31**, 515-524, doi: 10.1177/1045389X19891624.
[15] L. Lin, Q. Zhou, M. Li, *Polym. Sci. Ser. A*, 2019, **61**, 913-921, doi: 10.1134/S0965545X19080017.
[16] B. K. Kim, S. Y. Lee, *Polymer*, 1996, **37**, 5781-5793, doi: 10.1016/S0032-3861(96)00442-9.
[17] J. D. Merline, C. P. R. Nair, C. Gouri, R. Sadhana, K. N. Ninan, *Eur. Polym. J.*, 2007, **43**, 3629-3637, doi: 10.1016/j.eurpolymj.2007.05.032.
[18] M. Babaahmadi, M. Sabzi, G. R. Mandavinia, M. Keramati, *Polymer*, 2017, **112**, 26-34, doi: 10.1016/j.polymer.2017.01.074.
[19] Y. Chen, D. C. Lagoudas, *J. Mech. Phys. Solids*, 2008, **56**, 1766-1778, doi: 10.1016/j.jmps.2007.12.004.
[20] J. Diani, Y. Liu, K. Gall, *Polym. Eng. Sci.*, 2006, **46**, 486-492, doi: 10.1002/pen.20497.
[21] Y. Liu, K. Gall, M. L. Dunn, A. R. Greenberg, *J. Diani, Int. J. Plasticity*, 2006, **22**, 279-313, doi: 10.1016/j.ijplas.2005.03.004.
[22] Y. Feng, M. Bodaghi, W. Liao, *J. Appl. Polym. Sci.*, 2019, **136**, 47422, doi: 10.1016/j.mechmat.2019.01.004.
[23] J. Gu, J. Leng, H. Sun, H. Zeng, Z. Cai, *Mech. Mater.*, 2019, **130**, 9-19, doi: 10.1016/j.mechmat.2019.01.004.
[24] Q. Yang, FEM Numerical Simulation for Constitutive Model of Shape Memory Polymers based on Viscoelstic Theory, Tongji University, Shanghai, 2007.
[25] H. Qi, T. D. Nguyen, F. Castro, C. M. Yakacki, R. Shandas, *J. Mech. Phys. Solids*, 2008, **56**, 1730-1751, doi: 10.1016/j.jmps.2007.12.002
[26] V. Srivastava, S. A. Chester, L. Anand, *J. Mech. Phys. Solids*, 2010, **58**, 1100-1124, doi: 10.1016/j.jmps.2010.04.004.
[27] M. Nishikawa, K. Wakatsuki, A. Yoshimura, N. Takeda, *Compos. Part A-Appl. S.*, 2012, **43**, 165-173, doi: 10.1016/j.compositesa.2011.10.005.
[28] H. Yang, L.Wang, *Appl. Compos. Mater.*, 2013, **20**, 287-301, doi: 10.1007/s10443-012-9271-x.
[29] O. Soykasap, *Compos. Struct.*, 2009, **89**, 374-381, doi: 10.1016/j.compstruct.2008.08.012.
[30] Y. Liu, H. Sun, H. Tan, X. Du, *J. Appl. Polym. Sci.*, 2013, **127**, 3152-3158, doi: 10.1002/app.37688.
[31] V. A. Maidannyk, A. S. L. Lim, M. A. E. Auty, Y. H. Roos, *Food Res. Int.*, 2019, **116**, 1212-1222, doi: 10.1016/j.foodres.2018.10.008.
[32] J. C. Mauro, Y. Z. Mauro, *Physica A*, 2018, **506**, 75-87, doi: 10.1016/j.physa.2018.04.047.

Publisher's Note